Monthly Notices
of the
ROYAL ASTRONOMICAL SOCIETY

Mon. Not. R. Astron. Soc. **419,** 116–123 (2012) doi:10.1111/j.1365-2966.2011.19676.x

1H 0707−495 in 2011: an X-ray source within a gravitational radius of the event horizon

A. C. Fabian,[1⋆] A. Zoghbi,[1] D. Wilkins,[1] T. Dwelly,[2] P. Uttley,[2] N. Schartel,[3] G. Miniutti,[4] L. Gallo,[5] D. Grupe,[6] S. Komossa[7,8] and M. Santos-Lleó[3]

[1]*Institute of Astronomy, Madingley Road, Cambridge CB3 0HA*
[2]*School of Physics and Astronomy, University of Southampton, Highfield, Southampton SO17 1BJ*
[3]*XMM–Newton Science Operations Centre, ESA, Villafranca del Castillo, Apartado 78, E-28691 Villanueva de la Cañada, Madrid, Spain*
[4]*Centro de Astrobiologia (CSIC-INTA), Dep. de Astrofisica; LAEFF, PO Box 78, E-28691, Villanueva de la Cañada, Madrid, Spain*
[5]*Department of Astronomy and Physics, Saint Marys University, Halifax, NS B3H 3C3, Canada*
[6]*Department of Astronomy and Astrophysics, Pennsylvania State University, 525 Davey Lab, University Park, PA 16802, USA*
[7]*Technische Universität München, Fakultät für Physik, James-Franck-Strasse 1/I, 85748 Garching, Germany*
[8]*Excellence Cluster Universe, TUM, Boltzmannstrasse 2, 85748 Garching, Germany*

Accepted 2011 August 20. Received 2011 August 18; in original form 2011 July 15

ABSTRACT

The narrow-line Seyfert 1 Galaxy 1H 0707−495 went into a low state from 2010 December to 2011 February, discovered by a monitoring campaign using the X-Ray Telescope on the *Swift* satellite. We triggered a 100 ks *XMM–Newton* observation of the source in 2011 January, revealing the source to have dropped by a factor of 10 in the soft band, below 1 keV, and a factor of 2 at 5 keV, compared with a long observation in 2008. The sharp spectral drop in the source usually seen around 7 keV now extends to lower energies, below 6 keV in our frame. The 2011 spectrum is well fitted by a relativistically blurred reflection spectrum similar to that which fits the 2008 data, except that the emission is now concentrated solely to the central part of the accretion disc. The irradiating source must lie within 1 gravitational radius of the event horizon of the black hole, which spins rapidly. Alternative models are briefly considered, but none has any simple physical interpretation.

Key words: black hole physics – galaxies: individual: 1H 0707−495 – X-rays: galaxies.

1 INTRODUCTION

The narrow-line Seyfert 1 Galaxy 1H 0707−495 is bright in soft X-rays where it shows the steep spectrum and rapid variability typical of its class. *XMM–Newton* observations revealed a sharp drop in its spectrum around 7 keV, which can be interpreted either as an iron absorption feature or as the blue wing of a large broad emission line (Boller et al. 2002; Fabian et al. 2002). Further observations showed the drop to shift to a higher energy (Gallo et al. 2004), possibly due to ionization changes. A 500 ks *XMM* observation of 1H 0707−495 in 2008 provided clear support for the emission interpretation. A feature at 1 keV enables the spectrum to be decomposed into a power-law continuum with broad Fe-K and Fe-L emission lines (Fabian et al. 2009). These are expected from the irradiation of an iron-rich accretion disc around a black hole and are well fitted by a relativistically blurred reflection model (Fabian et al. 2009; Zoghbi et al. 2010).

High-frequency variations in the power-law continuum are followed about 30 s later by variations in the reflection component (Fabian et al. 2009; Zoghbi et al. 2010). Such reverberation and its spectrum (Zoghbi, Uttley & Fabian 2011) are fully consistent with, and expected from, reflection. The data indicate a rapidly spinning black hole of mass $M \sim 5 \times 10^6\,\mathrm{M}_\odot$ and spin $a > 0.97$. The power-law continuum originates from a corona close ($<10\,r_\mathrm{g} = 10\,GM/c^2$) to the black hole.

We report here on new *XMM* observations made in 2011 January in response to a prolonged drop in X-ray flux from 1H 0707−495 seen in a monitoring campaign of the source made with the X-Ray Telescope (XRT) on *Swift*. The spectrum shows the source at an unprecedented low level in the soft X-ray band. A reflection spectrum provides a good fit and requires that the power-law continuum source has moved to within a radius of $2r_\mathrm{g}$ of the black hole.

Alternative interpretations are briefly discussed. Deep *XMM*–RGS observations in 2008 show no evidence for a line-of-sight ionized wind or a warm absorber in this object (Blustin & Fabian 2009), and we do not pursue such models further here.

Other active galactic nucleui (AGNs) have been seen in a low state with strong reflection components (e.g. 1H 0419−577, Fabian et al. 2005; NGC 4051, Ponti et al. 2006; PG 1543+489, Vignali et al. 2008; Mrk 335, Grupe et al. 2008; PG 1535+547, Ballo et al. 2008; PG 2112+059, Schartel et al. 2010). The spectrum of 1H 0707−495 presented here has the most extreme relativistic parameters yet seen.

⋆E-mail: acf@ast.cam.ac.uk

2 *SWIFT*-MONITORING CAMPAIGN

During the period of 2010 March to 2011 March we monitored the X-ray and ultraviolet (UV) emission from 1H 0707−495 using the *Swift* satellite in order to improve measurements of the low-frequency power spectrum of the source. An ∼1 ks observation was obtained every ∼4 d. In some cases, due to observational constraints, the 1 ks exposure time was split into two or more short subexposures (visits). We used an automated script to download the *Swift*–XRT data from the HEASARC quick look website[1] shortly after they were obtained. The *Swift*–XRT data were then processed and reduced through our automated pipeline, which combines a mixture of standard HEASOFT tools[2] and some of our own routines. We outline the pertinent steps of our pipeline below. First, the raw *Swift*–XRT data are reprocessed with the XRTPIPELINE tool (version 0.12.6) to produce a calibrated and cleaned events file. A zeroth-order measure of the count rate is obtained by constructing a light curve (using the XSELECT tool) from the counts detected within a 30 arcsec radius aperture centred on the nominal position of 1H 0707−495. Following the method of Evans et al. (2007) we then maximize the signal-to-noise ratio by using an adaptively sized aperture which is chosen to give the highest quality measurements of the the source count rate. The radius of the optimally sized circular aperture is determined from the zeroth-order brightness and for 1H 0707−495 ranged between 17 and 45 arcsec. The background is estimated by measuring the count rate within an annular region surrounding the target aperture and is subtracted taking account of the relative areas of the source and background regions. The effective area of *Swift*–XRT is strongly sensitive to the location of the source within the image plane and to the specific extraction aperture used. The following procedure is used to normalize the raw count rate. First, the XRTMKARF tool is used to calculate an ancillary response function (ARF) file for each visit, taking account of the exposure map at the location of the source and the aperture size used. Using this ARF together with the standard XRT response matrix, and adopting a spectral model of a $\Gamma = 3$ power law absorbed by the Galactic column, we generate a fake visit spectrum using XSPEC. We then calculate the appropriate normalization factor by dividing the count rate of the faked visit spectrum by the count rate expected from a faked spectrum generated using the nominal instrumental ARF. Using the faked spectrum associated with the nominal ARF we calculate an approximate normalized count rate to flux conversion factor of 0.366 count s^{-1} $(10^{-11}$ erg cm^{-2} $s^{-1})^{-1}$ for the 0.5–10 keV band. Uncertainties on count rates are estimated assuming Poisson statistics, following the method of Gehrels (1986). Note that during a number of visits, the target position landed directly on, or very close to, one of the several bad columns on the XRT detector. In these cases the normalization factor is somewhat uncertain, and so we have added in quadrature a systematic uncertainty of 25 per cent.

The progress of the *Swift* monitoring was checked regularly, and we noted early in 2011 January (around MJD 55570) that 1H 0707−495 had become exceptionally faint in the X-ray band. A *Swift* ToO request was then initiated with daily monitoring of 1H 0707−495, which confirmed the prolonged dip in the X-ray brightness. A section of the 0.5–10 keV *Swift*–XRT light curve, bracketing the pronounced dip in the X-ray flux, is presented in Fig. 1.

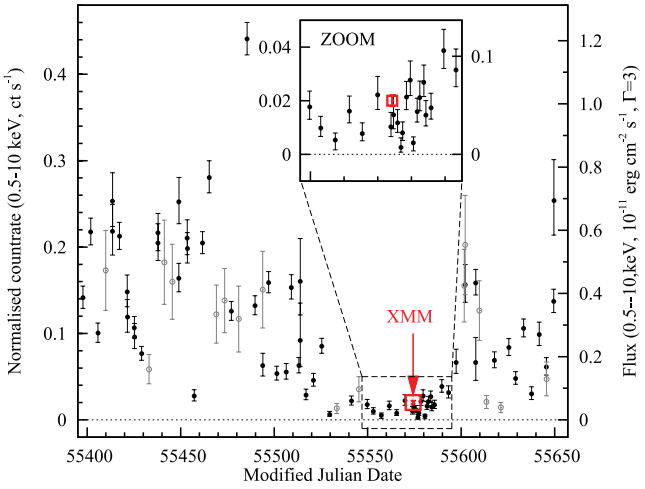

Figure 1. The *Swift*–XRT light curve for 1H 0707−495 showing the pronounced dip in X-ray brightness. Each point shows the normalized 0.5–10 keV count rate measured during a single *Swift*–XRT visit. An approximate flux scale is indicated, derived assuming a power-law spectrum with slope $\Gamma = 3$, and corrected for the Galactic column. A systematic uncertainty of 25 per cent has been added in quadrature to measurements where the target position landed on or near bad CCD columns (shown with open grey symbols). The epoch of the *XMM–Newton* observation is indicated with a vertical arrow.

The optical monitors on both *Swift* and *XMM–Newton* record the UV flux of the source. No marked change was seen during the observations (Cameron et al., in preparation).

3 *XMM–NEWTON* DATA FROM 2011

1H0707−495 was observed with *XMM–Newton* on 2011 January 12–13 (observation ID 0554710801) in large window mode for a total exposure of 100 ks. The observational data files were reduced using *XMM–Newton* science software SAS v11.0.0. There were some strong background flares during the observation, which were excluded in the spectral analysis, leaving a total net exposure of 65 ks. Standard filtering and event selection were applied. The source spectrum was extracted from a circular region of radius 35 arcsec centred on the source and background from the surrounding regions in the same chip. The spectra were then grouped using GRPPHA so that each bin had a minimum of 50 counts. The response files were generated using RMFGEN and ARFGEN. We show only pn data here for ready comparison to the 2008 analysis and since the pn has better sensitivity in the Fe-K band. The MOS data show good agreement with the pn results.

3.1 Model fitting

The *XMM–Newton* pn spectrum is shown in comparison to that of 2008 in Fig. 2. It is clear that there is a large, order of magnitude, drop in the soft flux below 1 keV, but only a factor of about 2 drop at 5 keV. In an $EF(E)$ spectral sense the hard flux peaks between 5 and 6 keV. Other *XMM* observations of the source give spectra lying between those of 2008 and 2011 (Fig. 2), but at least a factor of 3 above that of 2011 in the soft band.

We fit the 0.3–10 keV spectrum with a model similar to that used by Fabian et al. (2009) and Zoghbi et al. (2010), consisting of a relativistically blurred reflection component (convolution model KDBLUR acting on the ionized reflection model REFLIONX of Ross &

[1] http://swift.gsfc.nasa.gov/cgi-bin/sdc/ql
[2] http://heasarc.gsfc.nasa.gov/docs/software/lheasoft/

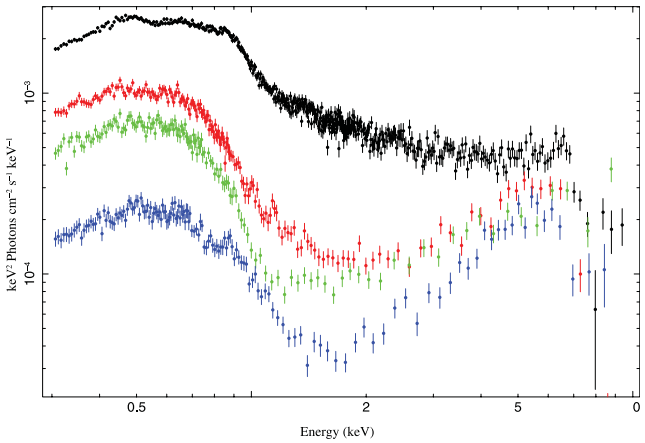

Figure 2. *XMM* pn spectra of 1H 0707−495 in 2008 (black, upper), 2000 (red), 2007 (green) and 2011 (blue, lower).

Table 1. Values of model parameters used in emisivity profile determination. The model used is `phabs*zphabs*(blackbody+kdblur*atable{reflionx.mod})`. The two absorption components have a fixed Galactic value and a variable intrinsic one, respectively. Representative values from fits to the total 2008 data (Zoghbi et al. 2011) are listed in the last column for comparison with the new results. The source varied considerably during the 500 ks observation.

Component	Parameter	Value	2008
Absorption	Galactic $N_{\rm H}$ cm^{-2}	4.3×10^{20}	
	Intrinsic $N_{\rm H}$	7.1×10^{20}	
Power law	Photon index, Γ	$2.71^{+0.1}_{-0.07}$	3.2
	Norm	$<1.3 \times 10^{-5}$	1.1×10^{-3}
KDBLUR	Inclination, i°	$69.3^{+1.2}_{-2.2}$	58.5
	$R_{\rm in}\, r_{\rm g}$	<1.3	1.23
	Index, q	>8.6	6.6
Blackbody	temperature, kT keV	$0.030^{+0.01}_{-0.007}$	0.037
	Norm	$5.7^{+25}_{-4.9} \times 10^{-4}$	2.1×10^{-3}
REFLIONX	Iron abundance / solar	>7.2	>7
	Ionization parameter, ξ erg cm s^{-1}	$12.7^{+2.8}_{-1.7}$	57
	Norm	$1.5^{+0.9}_{-0.6} \times 10^{-5}$	5.1×10^{-5}
	Redshift, z	4.06×10^{-2}	
χ^2/dof	317/340		

Fabian 2005) and a low-temperature blackbody. Absorption by a Galactic column density of 4.3×10^{20} cm^{-2} (Kalberla et al. 2005) is applied and intrinsic cold absorption is allowed in the fitting process. The blackbody emission is only important below 0.5 keV. There is no evidence of the direct power-law continuum. The parameters of the model are given in Table 1 and the fit is shown in Fig. 3. (The MOS data give consistent results.) Overall, the parameters are similar to those fitting the 2008 data, except that the photon index Γ is flatter and the inclination is $\sim 10^\circ$ larger. The strong contribution of iron emission to the spectrum is demonstrated in Fig. 4, which was obtained by dropping the iron abundance in the model to its lowest value, 0.1, plotting the ratio of the data to the model. Strong broad Fe-K and Fe-L lines are again evident.

It is plausible that the photon index can change between observations, but not that the inclination can vary significantly, for such an inner region immediately around the black hole. Examination of the spectrum shows that the previous inclination of around 58° is

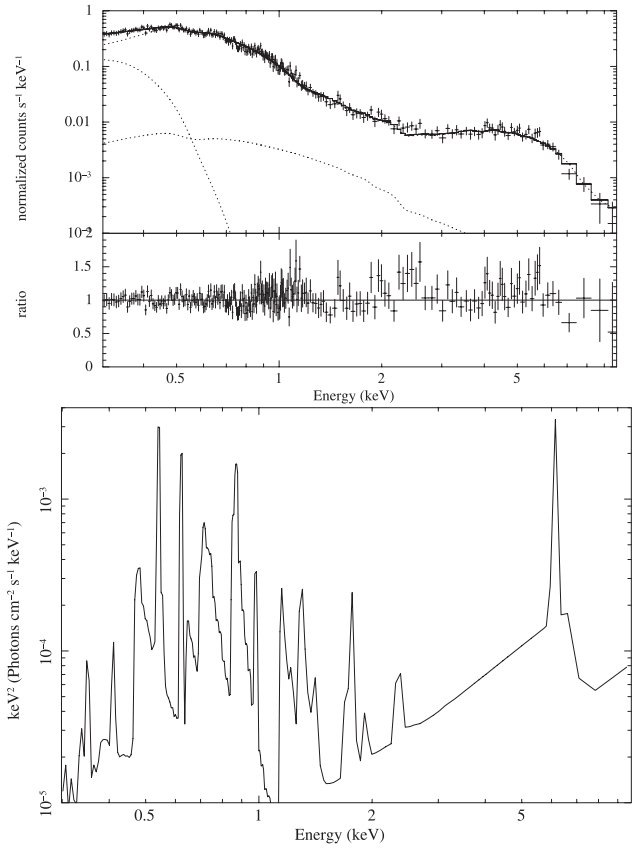

Figure 3. Top: *XMM* pn spectrum from 2011 with the best-fitting model consisting of a blurred reflection component, power-law continuum (the best-fitting amplitude is shown but the data are consistent with zero) and soft blackbody (see Table 1 for details). Lower panel: an unblurred reflection model.

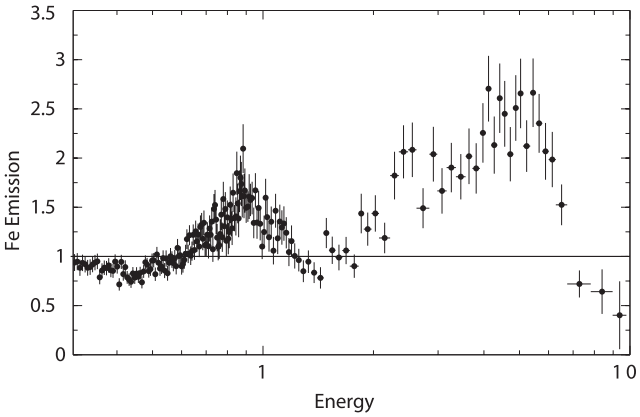

Figure 4. Contribution of iron emission to the single-reflector model. Note the strong contributions at both Fe-K and Fe-L lines.

the best fit for the new data above 1.5 keV. The higher inclination is driven by a slight excess around 1 keV. As seen in the lower panel of Fig. 3, the reflection is complex in this region. Inclusion of another reflection component with the same parameters as the first except for a higher ionization parameter $\xi = 990^{+1340}_{-140}$ erg cm s^{-1} provides a better fit ($\chi^2 = 308/337$; Fig. 5). It yields an inclination of $57.^\circ6 \pm 2.^\circ5$, very close to that indicated by the 2008 results. We interpret this to mean that the surface of the disc has regions of different density. (The best fits to the 2008 data also required a similar

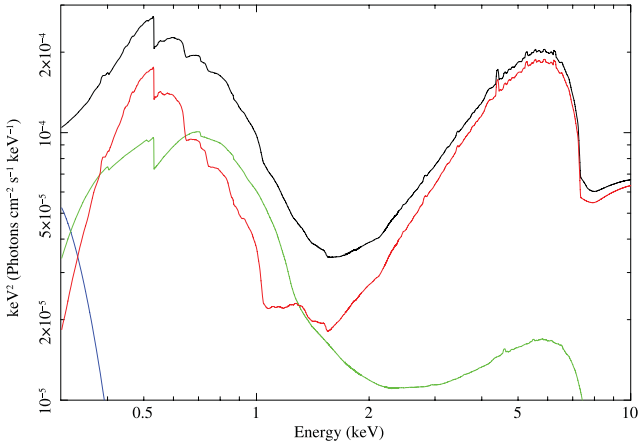

Figure 5. Double-reflector model. The high-ionization component is in green and the low-ionization component is in red. The reflectors differ only in ionization parameter and normalization.

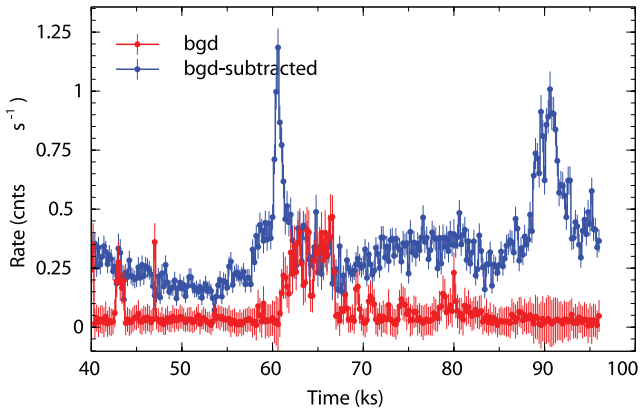

Figure 7. Light curve of the whole band from the pn detector, with 200 s binning, over the interval showing the highest flares. The background count rate of a larger spatial region, scaled to the extraction region used for 1 H0707−495, is shown in red.

additional high-ionization component, Fabian et al. 2009; Zoghbi et al. 2010.)

The above fits use the relativistic-blurring kernel KDBLUR for straightforward comparison to earlier work. The inner radius measured indicates the extent of gravitational redshift required by the spectrum. The relativistic-blurring code KERRCONV enables us to measure the black hole spin, for which we obtain $a > 0.997$, similar to that found by Fabian et al. (2009) and Zoghbi et al. (2010). The emissivity index of the reflection then has $q \sim 6.4$. The assumption made in determining the spin in this way is that the inner radius, $r_{\rm in}$, from which reflection is detected corresponds to the innermost stable circular orbit (ISCO) around the black hole. The low value of ξ found for the dominant reflection component means that the disc within $2r_{\rm g}$ is dense, and thus spatially thin. Under those conditions we expect that $r_{\rm in}$ is close to the ISCO (Reynolds & Fabian 2008). Matter falling inside the ISCO on plunge orbits quickly drops to a much lower density where it becomes completely ionized, so producing no iron reflection features.

3.2 Timing and variability

A light curve of the whole observation is shown in Fig. 6 in several energy bands, with a higher resolution (200 s bins) of the whole band in Fig. 7. The source continues to show rapid variability with several sharp spikes of emission. We see several instances where

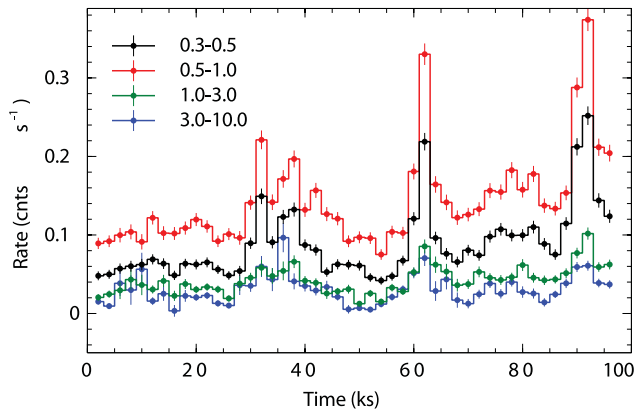

Figure 6. Multicolour X-ray pn light curves for the 2011 *XMM* observation.

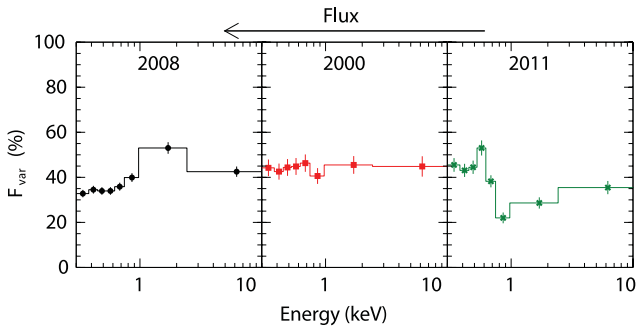

Figure 8. Fractional variability as a function of energy for three different observations of 1H 0707−495.

the emission rises and drops by a significant amount (factor of 2) on a time-scale of just a few 100 s.

The variability is more pronounced at lower energies. This is shown in Fig. 8, where the root-mean-square fractional variability is plotted and compared with that of earlier observations. The count rate is too low to make separate fits to the variations in 2011. The drop in fractional variability around 0.9 keV evident in Fig. 8 has two possible interpretations.

First, the flux could be low enough for a thermal component in the host galaxy to be relevant. In this case (narrow) Fe-L line emission would be significant at this energy and such a spatially extended component would not vary. A thermal component is not, however, required by spectral modelling. (The count rate is too low for any meaningful RGS analysis.) Secondly, the two-component reflector model allows for spectral variability if the components vary on different time-scales. Since the higher ionization component dominates over the 0.7–1.2 keV band, it seems that this is the less variable one. We have therefore investigated a model in which the ionization parameter of the lowly ionization component varies up to $\xi = 15\,{\rm erg\,cm\,s^{-1}}$. The fractional change is shown in Fig. 9. The model is not a fit. We do not pursue this further as more parameters could vary (both values of ξ, normalizations, Γ etc.) in possibly complex and related ways, but the trend is remarkably similar to the observed values.

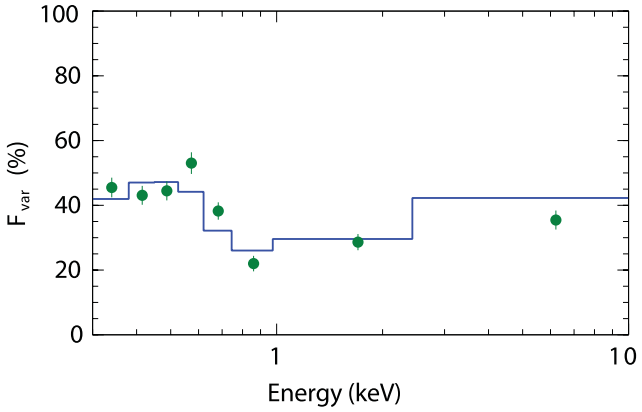

Figure 9. Fractional variability from 2011 observation plotted with the model in which the variability is due to ionization changes in the lowly ionized reflection component.

4 LIGHT-BENDING INTERPRETATION

Our results show that most of the reflection originates from within a radius of $2r_g$ where strong gravitational light bending must occur, enhancing the strength of the reflection component relative to the direct continuum (Martocchia & Matt 1996; Miniutti & Fabian 2004). We now examine what this means for the location of the primary source.

The iron-line emissivity profile of the accretion disc during the observation was obtained by fitting the photon counts (normalizations) of relativistically broadened emission lines (from the single REFLIONX X-ray reflection model convolved with the KDBLUR relativistic blurring kernel) originating from successive annuli in the accretion disc to the observed iron K line in the reflection spectrum (Wilkins & Fabian 2011). The emissivity profile is approximated by a power law with a steep index of around 8 (Fig. 10). Further weak emission beyond $5r_g$ with an index of between 3 and 4 over the outer regions of the disc is possible but is poorly constrained. The results are consistent with fitting a single, broadened, emission-line profile with a power-law emissivity profile over the entire disc. The steep fall-off in emissivity over the inner part of the disc results in the flux emitted from the outer disc regions being low, so the emissivity profile is less well constrained here. The emissivity profile has changed substantially from that found in *XMM–Newton* EPIC pn spectra obtained in 2008 January (Wilkins & Fabian 2011), where fitting reflection from successive annuli in the accretion disc suggested a twice-broken power-law form for the emissivity profile, with a steep index of 7.8 out to a radius of $5r_g$, where the profile flattened to an index of zero out to around $30r_g$ before tending to an index of 3 over the outer regions of the disc. Now almost 80 per cent of the emission originates from within $2r_g$, compared with 50 per cent from that region in 2008 (see Fig. 10). The conclusions are little changed if the emissivity index for the double-reflector model ($q = 6.5$) is adopted.

The emissivity profiles are compared to theoretical predictions obtained from ray-tracing simulations. Rays are traced from an isotropic point source at a height h above the plane of the accretion disc, either at rest on the rotation axis or offset from the axis, corotating with the disc below. Rays are traced from the source in the Kerr space–time around the central black hole, until they reach the accretion disc in the equatorial plane, where their positions and redshifts are recorded. The emissivity profile is found by counting the total (redshifted) energy of rays landing in each bin, which

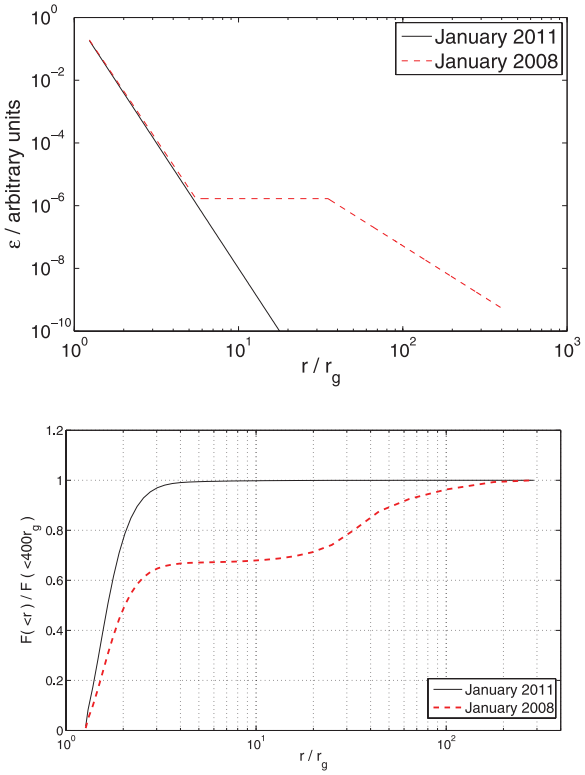

Figure 10. Top: emissivity versus radius for the single-reflector models fitting the spectra from 2011 (black) and 2008 (dashed red). Bottom: cumulative flux observed at infinity, as a function of disc radius, due to emissivity profiles shown in the top panel.

is proportional to the square of the redshift as both the energy of individual photons and photon arrival rates are affected. (The emissivity profile is defined as the power emitted from the disc per unit area.) The energy is divided by the area taking into account special and general relativistic effects due to the disc orbiting close to the black hole.

From the emissivity profile obtained from the 2008 January observation along with constraints from studying the X-ray variability and reverberation (Zoghbi et al. 2010), it would appear that the accretion disc is illuminated by an X-ray source close to the disc, while extending radially to around $20r_g$ (Fig. 11). Classically, the emissivity profile is expected to be flat in the region below the source where $r \ll h$, while tending to r^{-3} when $r \gg h$, where the flux received by the disc from the source falls off as the inverse square of the distance with a further factor of r arising from the cosine of the angle, projecting the ray normal to the disc plane. The reflected flux is enhanced over the inner region of the disc by relativistic effects where rays are focused towards the central black hole while photons are blueshifted travelling inwards and the space–time in the disc is warped, increasing the disc area, steepening the emissivity profile here.

The current observation, however, reveals an emissivity profile explained by a compact source, confined to a small region around the rotation axis and close to the black hole. The source is now required to be at a height less than $1.5r_g$ above the disc plane to explain the observed steepening over the inner region (Fig. 12). With the source this close to the black hole, there is no flattened region in the emissivity profile. Rather, the relativistic effects close to the black hole steepen the inner region of the profile out as far

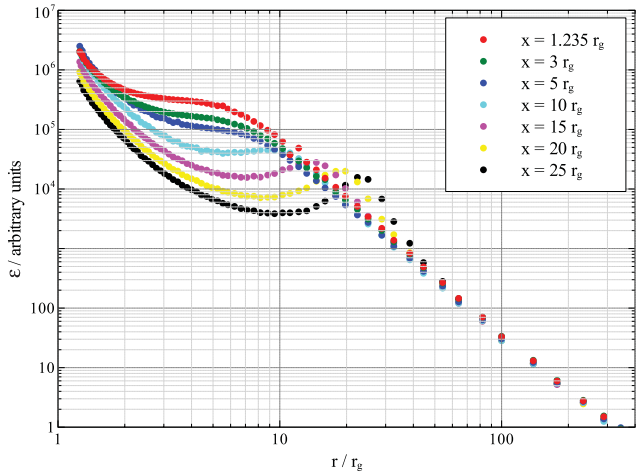

Figure 11. Theoretical emissivity profiles for point sources (equivalent to ring sources due to the axisymmetry of the spacetime) at a height of $5r_g$ with varying radius corotating with the disc below. In the context of these profiles, the twice-broken power-law emissivity profile obtained from the 2008 January observations can be understood in terms of an extended source at a low height above the disc which is formed from the sum of such profiles.

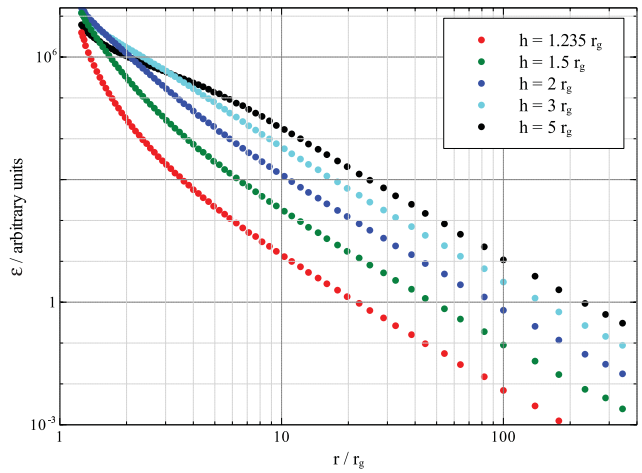

Figure 12. Theoretical emissivity profiles due to point sources at varying height on the rotation axis above the disc plane, suggesting that the once-broken power-law emissivity profile with the inner index 8 or more quickly changing to ∼6 and then to an index between 3 and 4 at a radius of $5r_g$ is produced by a primary source confined close to the rotation axis at a height less than $1.5r_g$.

as the region where $r \gg h$, so the emissivity profile takes the form of a once-broken power law from the steep inner profile to a profile slightly steeper than r^{-3} (with the slight steeping from the classical case due to rays being focused towards the black hole) over the outer regions of the disc. Ray-tracing simulations also illustrate the variation in the reflected flux observed compared to that in the power-law continuum as a function of the source height, by counting the photons in the simulation that hit the accretion disc compared to those which are able to escape to infinity (Fig. 13). A similar result is obtained when considering the variation in reflected and continuum flux as a function of source radius from the rotation axis. The substantial drop in the observed power-law continuum between the 2008 January observation and that of 2011 supports the hypothesis that the primary X-ray source has collapsed down to a region close to the black hole such that relativistic effects focus

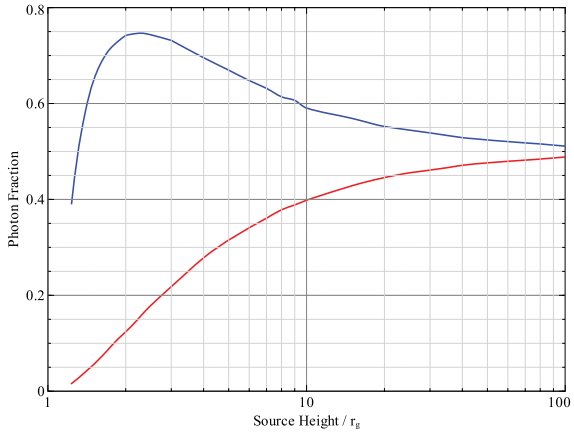

Figure 13. Fraction of photons escaping outwards (red lower curve) or inwards striking the disc (blue upper), determined from ray-tracing simulations.

the majority of the rays towards the black hole and on to the disc, so a greater fraction of the emitted X-rays are reflected from the disc, while very few are able to escape as part of the continuum. The source thus becomes reflection dominated.

5 ALTERNATIVE MODELS

The spectrum of the source is shown in Fig. 14 as a ratio to the power-law plus blackbody model which best fits over the energy range 0.3–6 keV (i.e. omitting the drop in the spectrum). The blackbody has a temperature of 0.123 ± 0.002 keV and the power-law index is $\Gamma = 0.35 \pm 0.04$. The spectral drop beginning at 6 keV is clear. The rest-frame energy of the neutral iron absorption edge at 7.1 keV is indicated by a dotted line in the figure and is above the energy of the observed drop. The spectral index of the power-law component, which dominates from 1.5 to 6 keV, is flatter than any plausible Comptonization process and so is not a reasonable solution.

The emission from 1.5 to 10 keV is well fitted by a Gaussian component with a central energy of $4.70^{+0.24}_{-0.34}$ keV and dispersion of $1.52^{+0.32}_{-0.23}$ keV (Fig. 14, upper centre). Next, a partial-covering solution is shown in Fig. 14 (lower centre) with $\Gamma = 2.33 \pm 0.06$. It requires 92 per cent covering by neutral gas of column density $N_H = 8 \times 10^{21}$ cm^{-2} with an iron abundance exceeding 80 times the solar value (90 per cent confidence level).

Both of these two models also require a blackbody component with a temperature of 0.116 ± 0.003 keV to account for the flux below 1 keV (χ^2/dof = 316/345 and 336/345 in the 0.3–10 keV band for the Gaussian and partial-covering models, respectively). This 'soft excess' component is common in the AGN and is unlikely to be a true blackbody associated, say, with the accretion disc since it shows a similar temperature over a wide range of object independent of black hole mass or accretion rate (Gierlinski & Done 2004; Crummy et al. 2006), contrary to the expectation of accretion theory. The simplest interpretation of such a (roughly) constant energy component is that it is due to atomic processes, in either absorption or emission. The lack of any sharp defining features requires that there is significant relativistic blurring which brings us back to strong reflection.

The strength of the drop at 6–7 keV, which requires a very extreme iron abundance (much higher than required to explain the earlier spectra; Boller et al. 2002), makes any partial-covering model

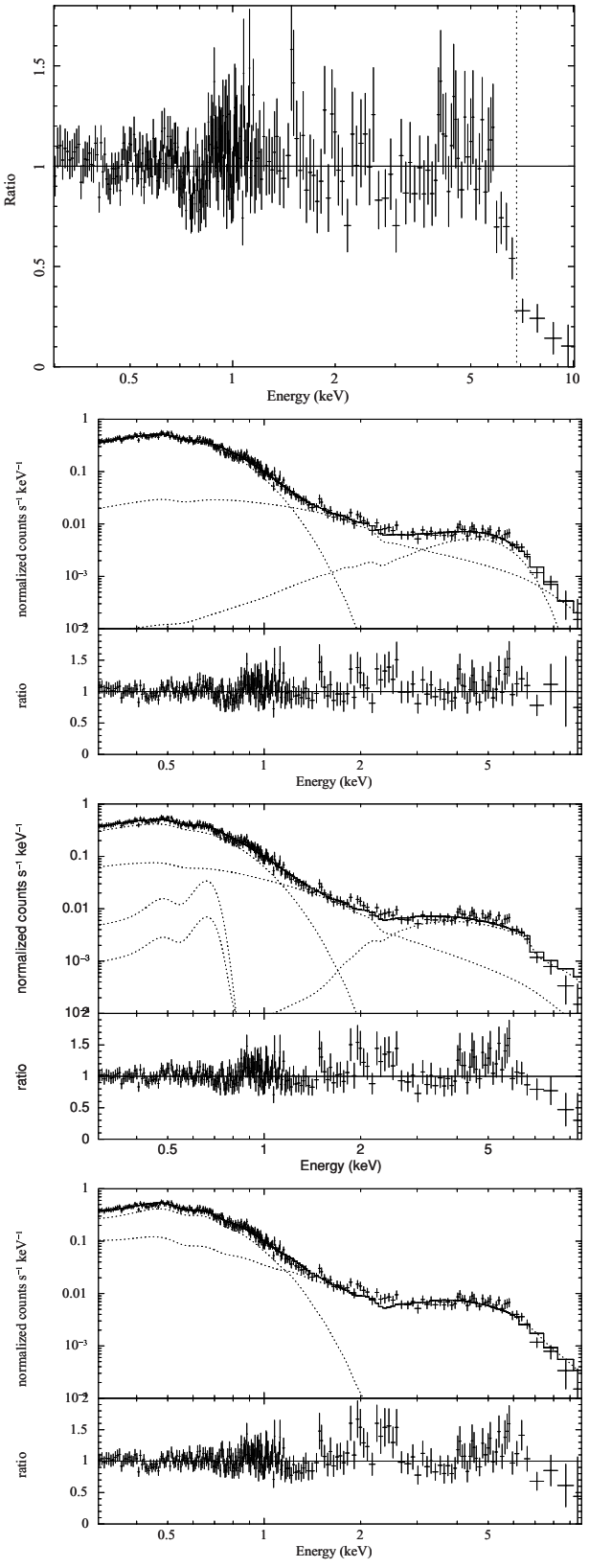

Figure 14. Top: the ratio of the 2011 *XMM* spectrum to a simple blackbody plus power-law model fitted over the band 0.3–5 keV. Upper centre: blackbody plus power-law and Gaussian model. Lower centre: partial-covering model; the absorbing column density is 8×10^{21} cm^{-2} and Fe abundance is 100. Bottom: the partially ionized absorber model. Note the poor fit above 5 keV.

implausible in our view. This model was also the worst fit, particularly in the 4–6 keV band.

A broad Gaussian component could be due to a down-scattered iron emission line, say from Fe XXV at 6.7 keV. To be down scattered to 4.7 keV requires about 40 Compton collisions (a Thomson depth of about 6), which would give a dispersion of about 0.4 keV. The fitted dispersion of 1.5 keV could then be explained by scatterer which is at $kT \sim 0.4$ keV. Such a medium would have to be completely ionized in order that it does not absorb the emission. This does not however explain the source of such an intense iron emission line in the first place, nor will it easily fit the previous observations.

Finally, a model with a power-law, $\Gamma = 2.87$, and blackbody components and two ionized absorbers (XSPEC model ZXIPCF $N_{\rm H,1} = 2.6 \times 10^{23}$ cm^{-2}, $\log \xi = 3.56$, $f = 1$; $N_{\rm H,2} = 2.2 \times 10^{23}$ cm^{-2}, $\log \xi = 1.79$, $f = 0.975$, where f is the covering fraction) can give a fair fit ($\chi^2 = 339$ for 343 d.o.f; Fig. 14, lower panel). The model has Fe-L and other absorption lines. No such lines or evidence for an ionized absorber were seen in the deep RGS spectrum from 2008 when the source was brighter (Blustin & Fabian 2009).

No absorber model for the bright state spectrum of 1H 0707−495 has yet accounted for the structure around both 7 keV and 1 in any self-consistent manner, such as is achieved with the blurred reflection model. Gallo et al. (2004), for example, added a Gaussian emission line at 0.92 keV. The spectrum we report on here appears to be just a more redshifted, and fainter, version of the bright state spectrum (Fig. 2). It does not make sense to us that the broad features in the low-state spectrum have a different physical origin to those in the high state.

5.1 An extended scattering region?

A major discovery from the 2008 *XMM–Newton* data was a ∼30 s soft lag found at high frequencies by Fabian et al. (2009) and Zoghbi et al. (2010). The lag was interpreted as the reverberation time delay due to the response of the reflection component, which dominated the soft flux (<1 keV), to variations in the power-law component, which is seen directly and dominates in the 1–3 keV band. Although the lack of any power-law component and low soft count rate precludes any lag analysis with the 2011 data, the interpretation is fully consistent with the unobscured, inner reflection, model which we use here to understand the 2011 spectrum.

Miller et al. (2010) have carried out a new timing analysis of the 2008 *XMM–Newton* data of 1H 0707−495. They confirm the ∼30 s soft lag but claim that the size of the lag at higher energies rules out the inner reflection model and instead propose that the source is surrounded by a ∼1000 light s radius scattering region. Holes are envisaged in the scattering cloud such that direct flux does emerge along our line of sight. We do not replicate their result using standard timing procedures, finding on the contrary that the spectral dependence agrees well with our model (Zoghbi et al. 2011). We are unable to check their approach since it uses a new, but as yet unpublished method.

Their model is motivated by the presence of a large positive low-frequency lag, in which the soft flux leads the harder flux. They argue that this is due to time delays in a large scattering cloud around the source. In their model, direct emission is seen dominating at soft energies below 1 keV, while the scattered/reflected flux dominates above that energy. No detailed model, which fits the spectral data, is presented by Miller et al. (2010), but we note that their direct and scattered/reflected components dominate in the soft and hard bands in the opposite way to those of the inner reflection model. Fabian et al. (2009) and Zoghbi et al. (2010) comment that the

low-frequency lags are similar to those commonly seen in Galactic binary black hole systems, where they are not due to scattering within a large cloud, and are likely to be due to accretion fluctuations propagating inwards in the disc and communicated to the central coronal structure by magnetic fields from a range of radii.

In a model in which scattering occurs in a 1000 light s radius cloud, then the power spectrum of the scattered/reflected component (hard band) should be steeply attenuated above 4×10^{-4} Hz, due to light traveltime smearing in the cloud, relative to the power spectrum of the direct component (i.e. the soft band). The observed power spectra however show exactly the *opposite* behaviour (see fig. 5 of Zoghbi et al. 2011). The soft bands have less high-frequency power than the hard bands, which show no sign of attenuation due to light traveltime effects; indeed, they even show an enhancement at higher frequencies. Finally, we note that recent discoveries of soft lags in other sources (De Marco et al. 2011; Emmanoulopoulos, McHardy & Papadakis 2011; Tripathi et al. 2011; Zoghbi & Fabian 2011; Zoghbi et al. 2011) support the inner reflection model for the 2008 data of 1H 0707−495 and argue against any special geometry or source inclination for such sources.

We infer that a model involving a large scattering cloud is an untenable interpretation of the *XMM–Newton* data of 1H 0707−495. The sharp changes in the light curve shown in Fig. 7 are strong evidence against any significant scattering cloud being present in 2011.

6 SUMMARY AND DISCUSSION

The low-state observation of 1H 0707−495 studied here shows a remarkable reflection-dominated spectrum and strong variability. We obtain a consistent solution to the degree of relativistic blurring required and the lack of a power-law component if the black hole is spinning very fast with the spin parameter $a > 0.997$, and the irradiating power-law source lies within $1r_{\rm g}$ of the black hole event horizon, i.e. at a radius of $2r_{\rm g}$ from the singularity. To our knowledge these are the first measurements *dominated* by emission from so close to the black hole.

The low-ionization parameter of the dominant reflection component means that the disc remains dense right to the innermost radii. This in turn implies that the disc remains thin. No strong poloidal magnetic fields are therefore expected, so there is unlikely to be any strong Blandford & Znajek (1977) effect.

Orban de Xivry et al. (2011) argue that the extreme properties of narrow-line Seyfert 1 galaxies as a class are due to the growth of their black holes, being dominated by internal secular evolution. This leads to prolonged gas accretion and high black hole spin.

The main reduction in the flux of 1H 0707−495, which is of an order of magnitude relative to 2008, occurs in the soft band, below 1 keV. The hard-band flux around 5 keV drops by only a factor of 2. Part of the soft-flux drop is due to a change in the spectral index of the irradiating continuum, from $\Gamma \sim 3$ to 2.4–2.7. The energy density in soft-disc photons incident on to the power-law source will change as it approaches the black hole. Assuming that the power-law emission is due to Comptonization from constant temperature electrons, Γ reduces (the source hardens) if the soft-photon energy density reduces. It is plausible that the energy density drops very close to the black hole, in support of our interpretation. We shall examine this further with future detailed calculations.

Several alternative interpretations of the low-state spectrum have been studied. None offers a simple physical and consistent interpretation.

ACKNOWLEDGMENTS

We thank the referee for a helpful report. ACF thanks the Royal Society for support. PU is supported by an STFC Advanced Fellowship and funding from the European Community's Seventh Framework Programme (FP7/2007-2013) under grant agreement number ITN 215212 'Black Hole Universe'. DG acknowledges support by NASA grant NNX09AN12G.

REFERENCES

Ballo L., Giustini L., Schartel N., Cappi M., Jiménez-Bailón E., Piconcelli E., Santos-Lleó M., Vignali C., 2008, A&A, 483, 137
Blandford R. D., Znajek R. L., 1977, MNRAS, 179, 433
Blustin A. J., Fabian A. C., 2009, MNRAS, 399, L169
Boller T. et al., 2002, MNRAS, 329, 1
Crummy J., Fabian A. C., Gallo L. C., Ross R. R., 2006, MNRAS, 365, 1067
De Marco B., Ponti G., Uttley P., Cappi M., Dadina M., Fabian A. C., Miniutti G., 2011, MNRAS, 417, L98
Emmanoulopoulos D., McHardy I. M., Papadakis I. E., 2011, MNRAS, 416, L94
Evans P. A. et al., 2007, A&A, 469, 379
Fabian A. C., Ballanytyne D. R., Merloni A., Vaughan S., Iwasawa K., Boller T., 2002, MNRAS, 331, L35
Fabian A. C., Miniutti G., Gallo L., Boller T., Tanaka Y., Vaughan S., Ross R. R., 2004, MNRAS, 353, 1071
Fabian A. C., Miniutti G., Iwasawa K., Ross R. R., 2005, MNRAS, 361, 795
Fabian A. C. et al., 2009, Nat, 459, 540
Gallo L. C., Tanaka Y., Boller T., Fabian A. C., Vaughan S., Brandt W. N., 2004, MNRAS, 353, 1064
Gehrels N., 1986, ApJ, 303, 336
Gierlinski M., Done C., 2004, MNRAS, 349, L7
Grupe D., Komossa S., Gallo L. C., Fabian A. C., Larsson J., Pradhan A. K., Xu D., Miniutti G., 2008, ApJ, 681, 982
Kalberla P. M. W., Burton W. B., Hartmann D., Arnal E. M., Bajaja E., Morras R., Pppel W. G. L., 2005, A&A, 440, 775
Martocchia A., Matt G., 1996, MNRAS, 282, L53
Miller L., Turner R. J., Reeves J. N., Braito V., 2010, MNRAS, 408, 1928
Miniutti G., Fabian A. C., 2004, MNRAS, 349, 1435
Orban de Xivry G., Davies R., Schartmann M., Komossa S., Marconi A., Hicks E., Engel H., Tacconi L., 2011, MNRAS, 417, 2721
Ponti G., Miniutti G., Cappi M., Maraschi L., Fabian A. C., Iwasawa K., 2006, MNRAS, 368, 903
Reynolds C. S., Fabian A. C., 2008, ApJ, 675, 1048
Ross R. R., Fabian A. C., 2005, MNRAS, 358, 211
Schartel N., Rodríguez-Pascual P. M., Santos-Lleó M., Jiménez-Bailón E., Ballo L., Piconcelli E., 2010, A&A, 512, A75
Tripathi S., Misra R., Dewangan G., Rastogi S., 2011, ApJ, 736, L37
Vignali C., Piconcelli E., Bianchi S., Miniutti G., 2008, MNRAS, 388, 761
Wilkins D. R., Fabian A. C., 2011, MNRAS, 414, 1269
Zoghbi A., Fabian A. C., 2011, MNRAS, in press (doi:10.1111/j.1365-2966.2011.19655.x)
Zoghbi A., Fabian A. C., Uttley P., Miniutti G., Gallo L. C., Reynolds C. S., Miller J. M., Ponti G., 2010, MNRAS, 401, 2419
Zoghbi A., Uttley P., Fabian A. C., 2011, MNRAS, 412, 59

This paper has been typeset from a TEX/LATEX file prepared by the author.